Short-term temporal changes in the characteristics of hydrothermal plumes at Rumble III volcano on the Kermadec arc, New Zealand

Anna Belcher

University of Washington School of Oceanography
Box 357940
Seattle
WA 98194-7940

acb206@u.washington.edu

May 2009

NON-TECHNICAL SUMMARY

The Kermadec arc, off the north east coast of New Zealand, hosts numerous submarine volcanoes. Many of these volcanoes are located at shallow depths, are highly active and are associated with hydrothermal plumes. Plumes rise buoyantly through the water column and "settle out" at a depth based on their density. The distribution of black smoker plumes can be mapped using a light scattering sensor to detect anomalously high particle concentrations. Variability in vent source conditions and the water column, in particular background currents, result in changes in plume distribution on short temporal scales. Therefore, it is difficult to obtain an accurate picture of plume dynamics based on a single "snapshot". Rumble III volcano on the Kermadec arc has a shallow summit (310 m), and rising hydrothermal plumes are strongly influenced by surface currents that vary over the tidal cycle. The unique shallow depth of Rumble III was utilized in this study to more easily and accurately investigate changes in plume distribution over the tidal cycle. Surveying occurred in March 2009, aboard the *R/V Thomas G. Thompson* as part of a student field course in collaboration with New Zealand scientists, Dr.Cornel de Ronde and Sharon Walker. Measurements with a conductivity-temperature-depth-optical (CTD-O) package revealed some of the highest particle anomaly signals ever recorded in a hydrothermal plume and were correlated with strong temperature anomalies. Background currents were quantified at Rumble III based on acoustic doppler current profiler (ADCP) analyses and used together with plume rise heights and temperature anomalies to document plume variability. The intensity, location and structure of plumes varied with the tides, highlighting the inaccuracy of characterizing a hydrothermal system based on one survey. Results have been used in concert with simple buoyant plume models to estimate previously unknown vent source conditions at Rumble III. The calculated heat flux (107 ± 7 MW) is over an order of magnitude greater than previous estimates, emphasizing the need to monitor hydrothermal vents to accurately estimate their contribution to the oceans heat budget.

ABSTRACT

Hydrothermal plumes are highly dynamic features, whose distribution varies on a range of temporal scales, from minutes to years. Plume variability can be caused by several mechanisms, including changes in vent source, background ocean stratification and current field. In March 2009, aboard the *R/V Thomas G. Thompson*, three conductivity-temperature-depth-optical (CTD-O) tow-yos were conducted at Rumble III volcano (35.75° S, 178.5° E) on the Kermadec arc, New Zealand, spanning different stages of the tidal cycle. The summit of Rumble III (310 m) places hydrothermal plumes within active surface currents. A hull-mounted acoustic current doppler profiler (ADCP) measured currents of 0.15 and 0.20 m s^{-1} at 330 m during ebb and flood flows respectively. Hydrothermal plumes were characterized by anomalies in nephelometric turbidity units (ΔNTU). This study documents the highest ΔNTU ever recorded at Rumble III, reaching 1.1 nephels. Three plume layers were measured near the volcano summit at water depths of 245, 350, and 420 m, and significant temperature (-0.38°C) and salinity (-0.11) anomalies were associated with the shallowest plume. Advection of plumes to the north and northwest, and changes in plume rise height between repeat tow-yo transects (~20 m), are consistent with oscillating tidal currents. Field measurements, combined with buoyant plume model predictions, provide new estimates of total vent source radius (0.22-0.33 m), temperature (200-400°C) and heat flux (107 ± 7 MW) at a source depth of 330 m at Rumble III. This heat flux is two orders of magnitude higher than previous estimates. The short-term variability of chemical and thermal fluxes suggests methods typically employed to characterize vent sites and estimate their contribution to global ocean heat budgets inadequately resolve temporal fluctuations.

INTRODUCTION

The Kermadec arc is part of the 2500 km Kermadec-Tonga arc-backarc complex formed by the convergence of Pacific and Australian plates (de Ronde et al. 2005). It is the longest submarine arc on Earth and submarine volcanoes have been documented along the entire length (Figure 1), many of which support intense hydrothermal plumes. Because of their importance to biogeochemical processes and heat and chemical transport (Lupton et al. 1995) hydrothermal vents are sites of considerable importance to biotic and abiotic ocean dynamics. Hydrothermal plumes of the Kermadec arc are fed by black and white smoker chimneys occurring at relatively shallow depths (~1650 to 200 m), which contrast typical depths of mid-ocean ridges (MORs) of 2200 to 2600 m (de Ronde et al. 2007). Rumble III (Figure 1) is one of these shallow volcanoes, with a summit that rises to approximately 310 m (Dodge 2009) making it a unique and important site for the study of hydrothermal systems.

Hydrothermal vent sites have complex chemistries and, despite extreme conditions, can host an abundance of life (Kelley et al. 2002). Plumes are a complex mix of dissolved chemical species and particulates (de Ronde et al. 2001). The dispersion of plumes and the chemical evolution of these systems over time have important implications for biological communities that are impacted by the dissolved and particulate plume components (Cowen et al. 2001). An understanding of the changes in plume dynamics and distribution therefore has a wider significance for the dispersion of chemical species and the potential for biological communities to survive.

Hydrothermal plume dynamics can be described based on physical idealizations. The hot vent fluid, up to 407 °C; (German et al. 2008), expelled from a vent, entrains cold water which dilutes the vent fluid by factors of $10^4 – 10^5$ (Lupton 1995). This entrainment increases the density of the plume as it rises, ultimately determining the height at which the plume is neutrally buoyant (see Figure 2).

Short-term hydrothermal plume variability

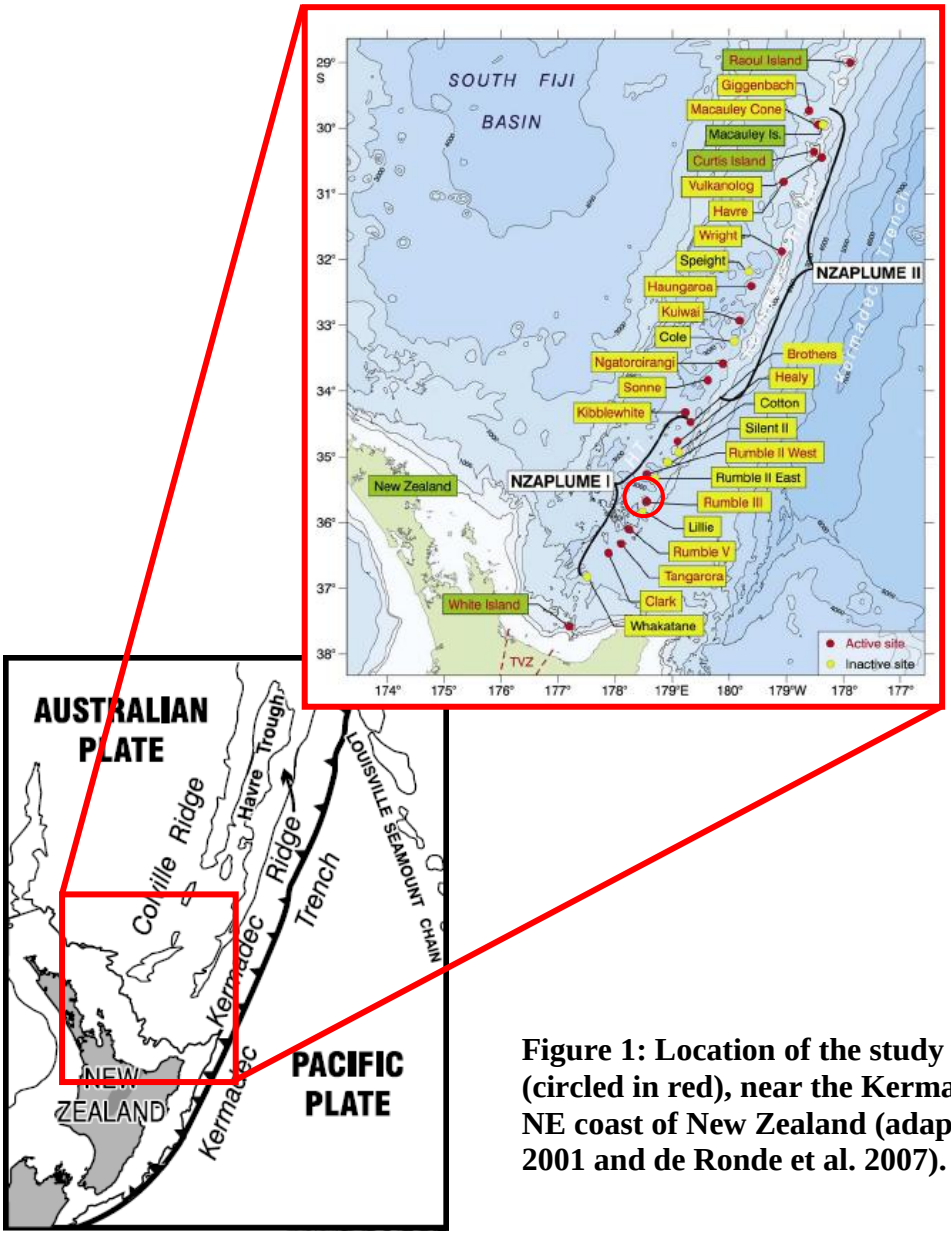

Figure 1: Location of the study site at Rumble III (circled in red), near the Kermadec Ridge off the NE coast of New Zealand (adapted from Wright 2001 and de Ronde et al. 2007).

Temperature and salinity characteristics of surrounding water strongly control the dynamics of the rising plume (Speer and Rona 1989). In the deep Pacific, salinity increases with depth, however, a salinity minimum occurs at 1000 m due to the presence of Antarctic Intermediate Water (Tomczak and Godfrey 1994). Hence, the surface region, in which Rumble III is located, exhibits a decrease in salinity with depth. A negative gradient of salinity in the ambient waters results in a neutrally buoyant plume that is cooler and fresher than the surroundings (Speer and Rona 1989). This is because once the rising plume has entrained enough cold water to remove the excess temperature the plume will be

fresher than the ambient water, giving it positive buoyancy. The freshness is a result of the entrainment and mixing of low salinity water from deeper in the water column (Rona and Speer 1989).

Theoretically, upon reaching neutral buoyancy, the plume will spread laterally along an isopycnal; however, the plume still possesses vertical momentum and may overshoot its level of neutral buoyancy. The resultant unstable plume is denser than the surrounding waters, has negative buoyancy, and therefore sinks and spreads at the level of zero buoyancy (Turner 1973). Eventually the neutrally buoyant plume settles at a particular density level determined by both the source and ambient conditions (Speer and Rona 1989).

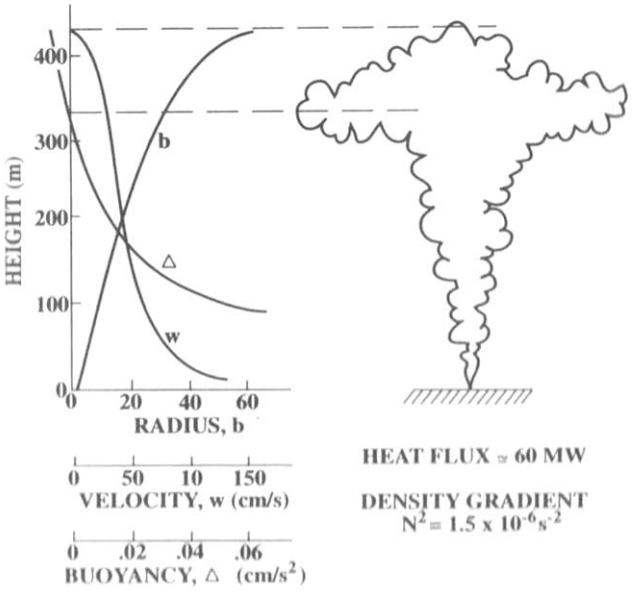

Figure 2: Schematic to show the dynamics of buoyant plume ascent in a stably stratified medium. The plot displays changes in plume radius (b), velocity (w) and buoyancy parameter (Δ) with height. The point of lateral spreading at neutral buoyancy is evident. Taken from Lupton (1995).

The maximum rise height of the plume can be predicted based on these physical characteristics (Speer and Rona 1989); however, there are many complications to this idealized view. For example, episodic activity causing variability in the vent source composition and flux will alter the rise of the buoyant plume, leading to temporal changes in the plume rise height (Rudnicki and Elderfield 1992).

Another simplifying approximation of many buoyant plume models is the absence of, or constant, crossflow. In contradiction to this assumption, studies have suggested tidal oscillations may cause significant changes in the rise height of hydrothermal plumes (Rudnicki and German 2002; Veirs et al. 2006). Rudnicki and German (2002) conducted continuous profiling of a nonbuoyant hydrothermal plume on the Central Indian Ridge. Although they recorded changes in plume rise height,

the plume was usually associated with a constant level of potential density. They suggest that bending of the plume by tidal currents may account for the periods when the plume deviated from this potential density level. Increased currents cause larger shear at the plume boundary and hence an increase in entrainment. The consequent rapid dilution of the plume leads to a faster decrease in buoyancy flux, and a lower maximum rise height (Middleton 1986). Currents effectively act to push the plume over, leading to changes in the measured rise height as background current velocities change on temporal scales of a tidal cycle (Rudnicki and German 2002).

Variability in plume position due to tidal currents is an area where extensive studies are lacking. This is mainly due the difficulty of obtaining a synoptic view of the entire plume at different stages of the tidal cycle. The deep locations of many submarine venting sites also introduce complexities into current measurement, making study both time consuming and costly. Rumble III's shallow depth provides an opportunity to easily collect accurate current velocity data at high temporal resolution, allowing more comprehensive investigation than has previously been possible at most vent sites. The shallow volcano summit also places hydrothermal plumes at depths that are influenced by variability in the surface current system, with predicted M2 and S2 tidal current velocities of 5.0 cm s^{-1} in the NW-SE direction (Egbert and Erofeeva 2002). This study is therefore able to document the short-term changes in the characteristics of hydrothermal plumes and examine the possible causes of variability.

Successful mapping of this short term variability requires real-time mapping of the plumes. A well established measure of deep-sea hydrothermal plumes is their associated temperature anomaly signals (Baker et al. 2003). However, temperature anomalies can be obscured by a non-linear background structure of temperature and salinity (Wilson et al. 1996). This is particularly true at depths shallower than 1200 m, as background temperature gradients of at least 0.01°C m^{-1} are likely to conceal temperature anomalies on the order of 0.1°C (Baker et al. 2003).

Short-term hydrothermal plume variability

Past studies at Rumble III have recorded hydrothermal plumes in the upper 300m of the water column, but temperature anomalies have not been resolved and optical backscatter is utilized to measure plumes (de Ronde et al. 2001; Baker et al. 2003). The plumes are enriched in both dissolved and particulate species, causing high optical anomaly signals that are suggestive of active venting (Baker et al. 2003). Particulate anomalies have been well correlated with other tracers of hydrothermal plumes such as dissolved manganese and helium, allowing even shallow plumes to be detected (Rudnicki and Elderfield 1992).

Although the location of hydrothermal plumes at Rumble III in the thermocline layer can inhibit the ability to resolve temperature anomalies, their location provides an exciting opportunity to investigate the effects of changing surface currents on the characteristics of a rising plume. The density gradient in this region is strong and hence small changes in background properties and episodic vent source activity could result in measurable changes in plume rise height. The objective of this study is to measure the short-term, tidal scale variability in the Rumble III plumes in terms of structure and rise height, and to determine the role of the ambient current profile on these changes. The buoyant plume model of Speer and Rona (1989) provides a valuable tool for determining key controls on hydrothermal variability. Each parameter can be changed in isolation and the resulting changes in the characteristics of the hydrothermal plume can be detected. In this way the combination of model simulations with field measurements allows for a more thorough and accurate investigation of hydrothermal plume variability and the processes acting on it.

METHODS

Fieldwork

Surveying of Rumble III, was carried out between 8-10 March 2009 aboard the *R/V Thomas G.*

Thompson (cruise TN230). Three conductivity-temperature-depth-optical (CTD-O) tow-yo transects (see Figure 3) were conducted at Rumble III to quantify characteristics of background ocean water and plumes, and to examine temporal variability on the scale of a tidal cycle. Camera tow surveys (using the TowCam system) were also conducted, in which the TowCam system was mounted with a CTD allowing for the detection of temperature spikes associated with venting.

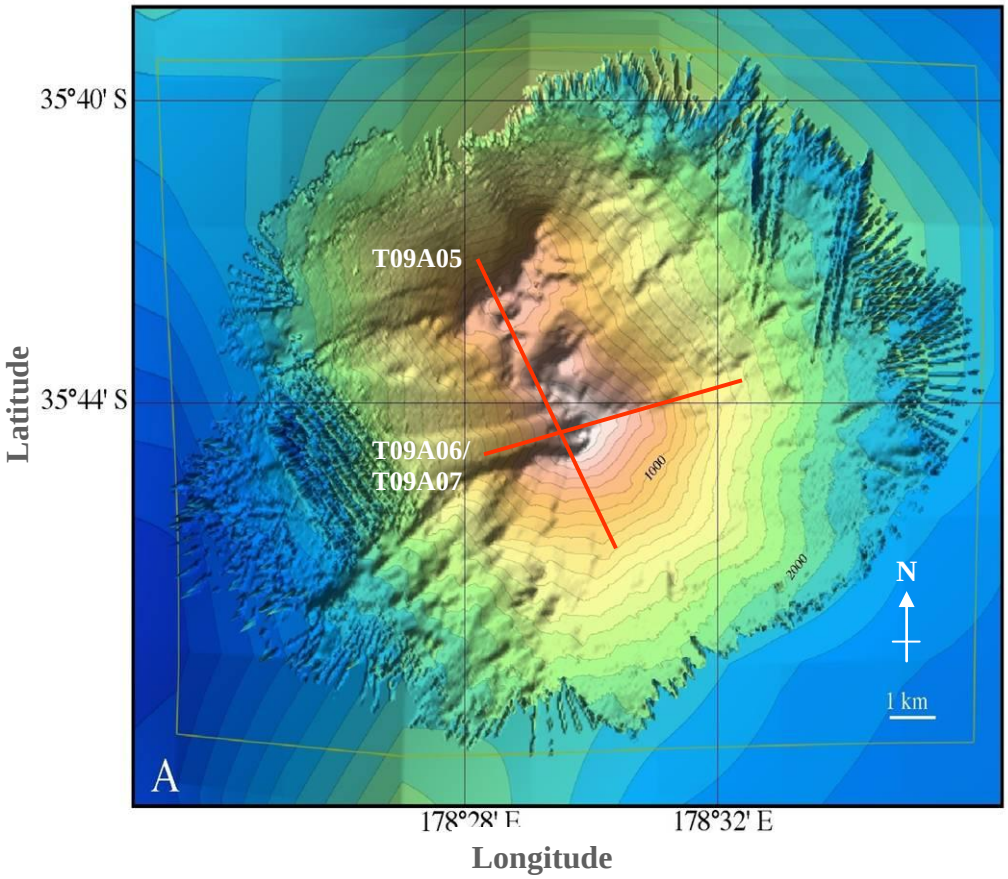

Figure 3: Bathymetric map showing the locations of CTD-O tow-yos over the summit of Rumble III. Bathymetry from Dodge (2009).

CTD-O tow-yos were carried out at different stages of the tidal cycle (Figure 4) as predicted by the OSU TPXO6 Tidal Model (Egbert and Erofeeva 2002). Temperature, and salinity data collected by the CTD-O package provided potential density measurements along the tow-yo paths. A Light Scattering Sensor (LSS) mounted on the CTD was used to define plume extent from the optical signal

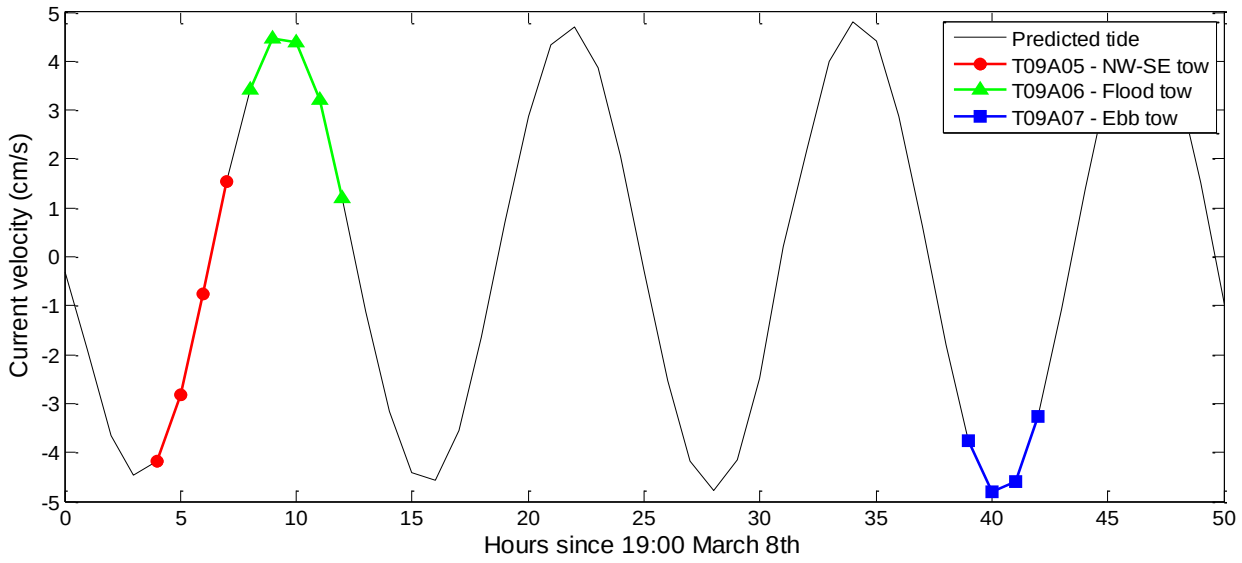

Figure 4: Predicted NW-SE tidal current velocities (cms-1) for the sum of tidal constituents M2, and S2, at Rumble III volcano (Lat: 35.87 S, Lon: 178.43 E) derived from the OSU Global Tidal Model (Egbert and Erofeeva 2002). Positive and negative values represent northwest and southeast flow respectively, i.e. flood and ebb tidal stages.

of their high particulate anomalies (Baker et al. 2003). The LSS measures the strength of the plume in terms of the arbitrary unit of nephelometric turbidity (NTU), or "nephels". Voltage data from the LSS was converted directly to NTU based on the calibration factor of the sensors after calibration with a solution of formazine (Walker. S. L. pers. comm.). The CTD-O package followed a sawtooth path with a wavelength of between 0.25 and 1.25 km depending on water depth and ship speed (~ 1.5 knots). During all transects, the hull-mounted 75 kHz RD Instruments ADCP recorded currents from 25 m to 650 m depth. Current velocity profiles, averaged over 5 minute intervals and separated into 8 m depth bins, were obtained from the ADCP using the University of Hawaii Data Acquisition System (UHDAS).

An initial survey of the site, CTD-O tow-yo T09A05, was carried out in the NW-SE direction to locate the position of hydrothermal plumes (Figure 1). The position of this CTD-O tow-yo was based on transects carried out during the 2002 New Zealand American PLUme Mapping Expedition (NZAPLUME) II cruise (Walker. S. L. pers. comm.). T09A05 was conducted during the ebb phase of

the tide, for which the OSU Global Tidal Model predicted maximum tidal currents of 4.2 cm s^{-1} to the southeast, decreasing during the tow (see Figure 4). Following this, two repeat CTD-O tow-yos, T09A06 and T09A07 were conducted in the SW-NE direction at maximum flood and maximum ebb, respectively (see Figures 3, 4).

Data Processing

ADCP data were filtered using Common Ocean Data Access System (CODAS) software to remove erroneous data. Where data have been removed, vertical interpolation using MATLAB were carried out and added to the data set. To produce stick plots of current velocities at a particular depth, an average was taken over ~25 m to further reduce any noise in the signal.

Particulate signals indicative of hydrothermal venting from LSS data were defined by the nephelometric turbidity anomaly (ΔNTU), a nondimensional optical standard;

$\Delta NTU = V_R - V_B$.

Here, V_R is raw voltage from the LSS and V_B is the voltage of background ambient water, i.e. water that has not been influenced by hydrothermal plumes (Baker et al. 2003). At Rumble III, a background value of 0.007 NTU was chosen based on the values recorded during the CTD-O tow-yos. Data were then extrapolated using the mapping software Surfer to produce a visual representation of 2D plume structure.

Temperature and Salinity Anomalies

Strong background gradients in temperature and salinity were recorded at the shallow depth of the plumes. However, by analyzing plume data over a small potential density interval of ~0.5kgm^{-3}, potential temperature and salinity values can be compared to the potential density by fitting a first order

polynomial to the background signal. The relationship is near linear in these focused regions, allowing temperature anomalies to be resolved. Only data with a ΔNTU <0.1 nephels were used to derive the polynomial equation to prevent biasing of the "background" profile by waters with a high plume signature. Temperature anomalies ($\Delta\theta$) have been calculated using the following formulae;

$$\Delta\theta = \theta_p - \theta_b,$$

where θ_p is the potential temperature of plume, and θ_b is the potential temperature of the background waters calculated as described above.

Computer Modeling

Model simulations using the Speer and Rona (1989) buoyant plume model were conducted to constrain vent source characteristics at Rumble III, based on field measurements. The buoyant plume model of Speer and Rona (1989) is adapted from that of Morton et al. (1956) and solves the vertical structure of potential temperature (θ), salinity (S) and vertical velocity (W) based on the effects of background stratification. The calculated values are averaged horizontally over the cross-sectional area (A) of the plume with A_0 defined by the vent source area. The equations of the model,

$$AW_z = EA^{\frac{1}{2}}W,$$
$$SAW_z = \bar{S}EA^{\frac{1}{2}}W,$$
$$\theta AW_z = \bar{\theta}EA^{\frac{1}{2}}W,$$
$$\rho_0 AW^2{}_z = -g(\rho - \bar{\rho})A,$$

are based on the conservation equations for mass, salt, heat and momentum, where g is the acceleration due to gravity, z is the depth, ρ is potential density, and E is the entrainment coefficient (0.255). An overbar denotes the background field, subscript 0 represents initial vent conditions, and the subscript z

is the vertical derivative. The model makes some simplifications that include assuming a steady plume and excluding the influence of background currents. The rise height (Z_{max}) calculated by the model satisfies;

$$Z_{\max} = 5Bo^{1/4}N^{-3/4}$$

where the buoyancy frequency (N), and buoyancy flux (Bo) are defined as;

$$N^2 = \frac{-g\ \alpha\bar{T}_z + \beta\bar{S}_z}{\rho},$$

$$Bo = -g\left[\alpha\ T_0 - \bar{T}\ + \beta\ S_0 - \bar{S}\ \right]A_0W_0.$$

Of the variables thus far undefined; α and β are coefficients of thermal expansion and saline contraction calculated from background hydrographic values (-2.0×10^{-4} and 7.5×10^{-4} respectively) and T is temperature (Speer and Rona 1989).

To estimate source conditions at Rumble III using this model, a number of assumptions were made based on current and previous studies. Background water stratification was estimated from the first downcast of T0907A (35.7445 S, 178.4701 E) because this cast was conducted over 2 km from the summit of Rumble III, where there was no optical evidence of hydrothermal venting. Initial source velocity was assumed to be 0.4 m s^{-1} based on a black smoker vent system in the TAG area of the Mid-Atlantic Ridge (Speer and Rona 1989). For simplicity, source salinity was assumed equal to background salinity at the source depth. De Ronde et al. (2005) estimate venting of 225 – 305°C at Brothers volcano on the Kermadec arc based on sulphide minerals at different sites (see Figure 1). These temperatures were used as a reasonable starting range and as a measure of realistic values for Rumble III. Recorded plume heights and temperature anomalies constrained the buoyancy of the emitted hydrothermal fluid and source depth, radius and temperature were varied to match field measurements.

Short-term hydrothermal plume variability

To determine whether the recorded differences in current velocity could explain variability in plume rise height, calculations were carried out using Middleton's (1989) case for a point source of buoyancy emanating into a stably stratified crossflow;

$$z = \left(\frac{6}{\alpha^2}\right)^{1/3} \left(\frac{F_s}{UN^2}\right)^{1/3}$$

F_s, U, and N denote the source buoyancy flux (m^4s^{-3}), crossflow velocity (ms^{-1}), and buoyancy frequency (s^{-1}) respectively. Middleton (1986) gives, $(6/\alpha^2)^{1/3} = 3.8$, based on laboratory observations. Values for source buoyancy frequency and flux were calculated based on source conditions derived from model simulations as described previously.

RESULTS

Current Profiles

ADCP data from T09A05, T09A06 and T09A07 show a variable background current field on tidal time scales (Figure 5). Tides in the region oscillate in the NW-SE plane with northwestward flood currents and southeastward ebb currents that reached peaks of 4.5 cm s^{-1} during the survey period. Subtracting tidal currents from the ADCP data using NIWA finite element tidal model (Walters et al. 2001) with software provided by Philip Sutton (pers. comm.), reveals a north to northwestward mean background current flow. This agrees with OSCAR (Ocean Surface Current Analyses – Realtime) satellite data (Bonjean and Lagerloef 2002) at the time of surveying.

Currents during T09A05, the NW-SE tow, were predominantly to the northwest except for a region of southeastward flow close to the volcano flanks at ~ 450 m depth (Figure 5A). There is a wedge of faster flowing northwestward currents in the upper 300 m of the water column, particularly to the south of the volcano between 50 m and 150 m depth where flow reaches about 0.38 m s^{-1}. In the region where plumes were detected, currents are on the order of 0.15 m s^{-1}.

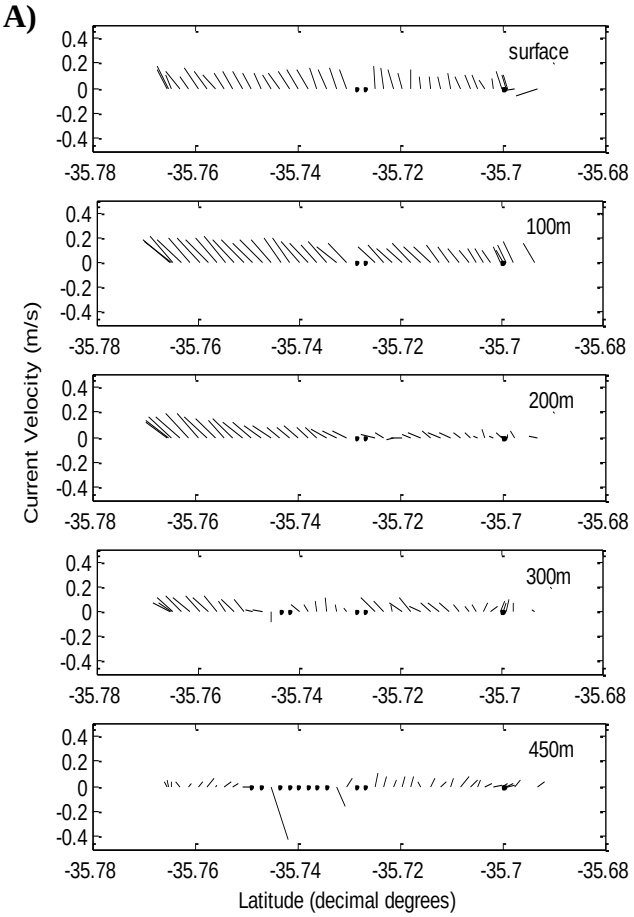

Figure 5: Stick plots displaying current velocity (m s^{-1}) and direction for A) T09A05, B) T09A06, and C) T09A07. Transects T09A06, T09A07 are displayed from west to east and T09A05 from south to north. Currents are shown at a number of depth levels and have been averaged over a small depth range to reduce noise; surface (20-40 m), 100 m (101-125 m), 200 m (205-229 m), 300 m (301-325 m), and 450 m (438-470 m). The lower limit of data defines the volcano summit and flanks and additional data gaps are where data were highly erroneous. The direction of sticks shows the current direction with respect to north and the length corresponds to the magnitude as marked on the vertical axis.

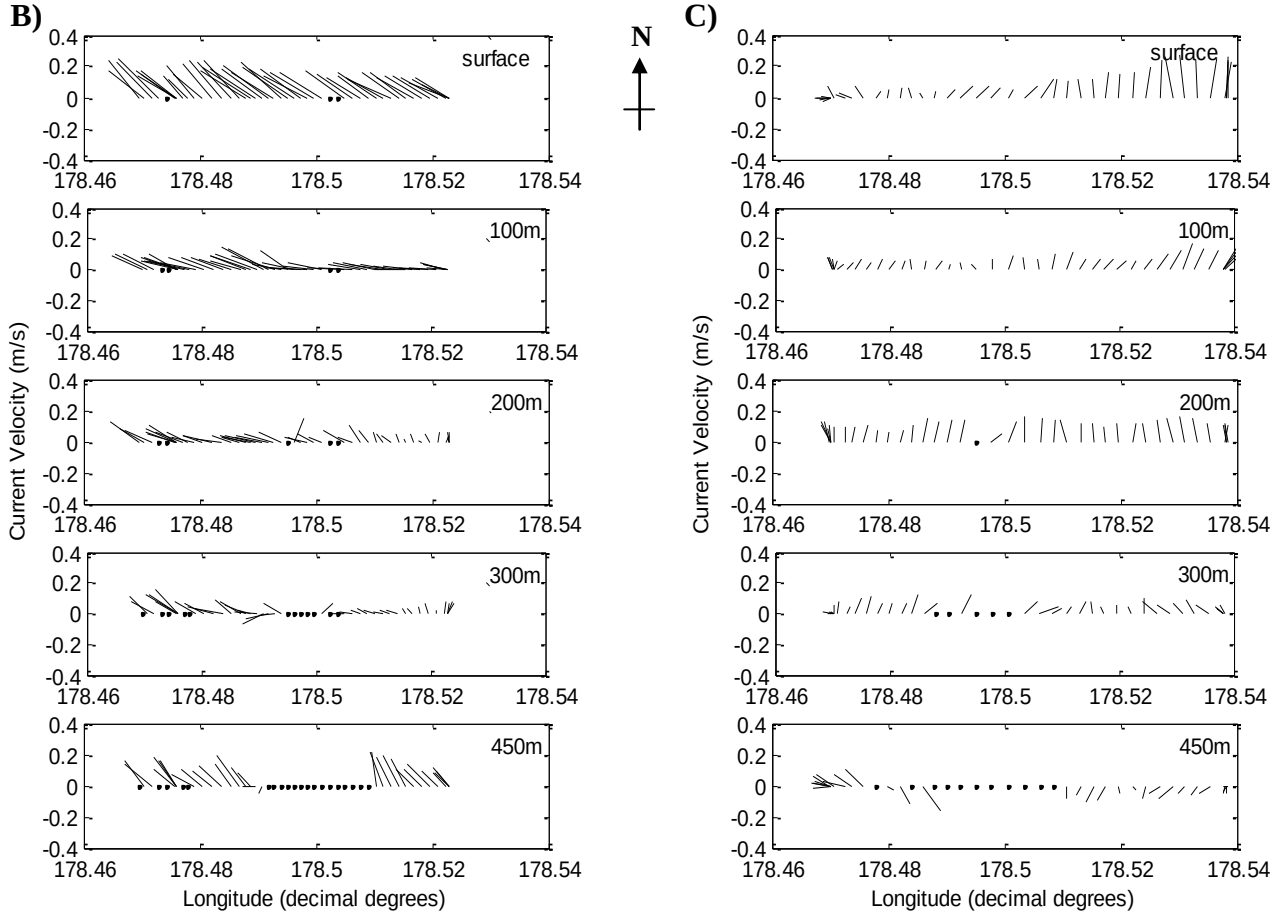

Short-term hydrothermal plume variability

Higher current velocities were recorded during T09A06 when tidal currents were in phase with the northwestward mean flow (Figure 5B, C). Strong currents are evident in Figure 5B, in particular to the west, in the top 100 m with maximum velocities of approximately 0.4 m s^{-1} at 80 m. Flow surrounding the volcano flanks appears to be quite vertically homogenous during T09A06, and northwestward flow dominates at all depths shown. The area above the summit of the volcano where plumes were detected (150-300 m) is characterized by northwestward currents of about 0.2 m s^{-1}.

Unlike T09A06, surface current velocities measured during T09A07 were not significantly elevated over deeper currents; with typical velocities of about 0. 1 m s^{-1} in a northward direction. The water column within 200 m of the summit (where optical plume signatures were detected) is characterized by currents of about 0.15 m s^{-1}. This is 0.05 m s^{-1} lower than those recorded in the same region during tow T09A06.

Plume Distribution

Nephelometric anomaly (ΔNTU) values of greater than 0.004 NTU (a reasonable threshold for the plume boundary; (Walker. S. L. pers. comm.) were recorded during each of the CTD-O tow-yos. Three plume layers were apparent at Rumble III but there was variation in both the plume strength and structure between tow-yos (Figure 6). Extrapolation of these data has caused some dampening of the high ΔNTU values and regions where data are lacking must be viewed critically. Extrapolation does however provide a tool for visualizing the plumes. One feature that is common among all three tows is the presence of a high optical backscatter layer in the top 200 m due to euphotic production (Baker et al. 2003). Background ΔNTU decreases to a mid water column minimum before increasing again to a bottom nepheloid layer associated with the bottom topography. High optical backscatter signals associated with hydrothermal venting are overlain on this background profile. When interpreting

profiles it is important to note that suspended sediment near the volcano flanks results can give the false impression of plumes. The use of a log scale means these anomalies appear more prominent above the background ΔNTU, but these regions can be identified by their proximity to the topography and by a low optical anomaly.

T09A05

This NW-SE tow shows evidence of a strong plume signature above the summit, with two strong centers of high optical backscatter at ~ 250 m and 270 m (Figure 6A) but elevated plume signals between 310 m and 210 m depth. The plume centers sit at potential density levels 26.35 and 26.41 respectively. This pattern could be explained by the rising of a single plume downstream. The maximum ΔNTU recorded was 0.234 nephels at a depth of 265 m, approximately 45 m above the volcano. A weaker plume signature, 0.04 nephels, was detected just to the southeast of the summit at about 325 m depth, at the 26.54 potential density contour. During the initial part of the survey the CTD was not raised above a depth of 450 m (Figure 6A); however, it is likely that a plume signature would

A) T09A05

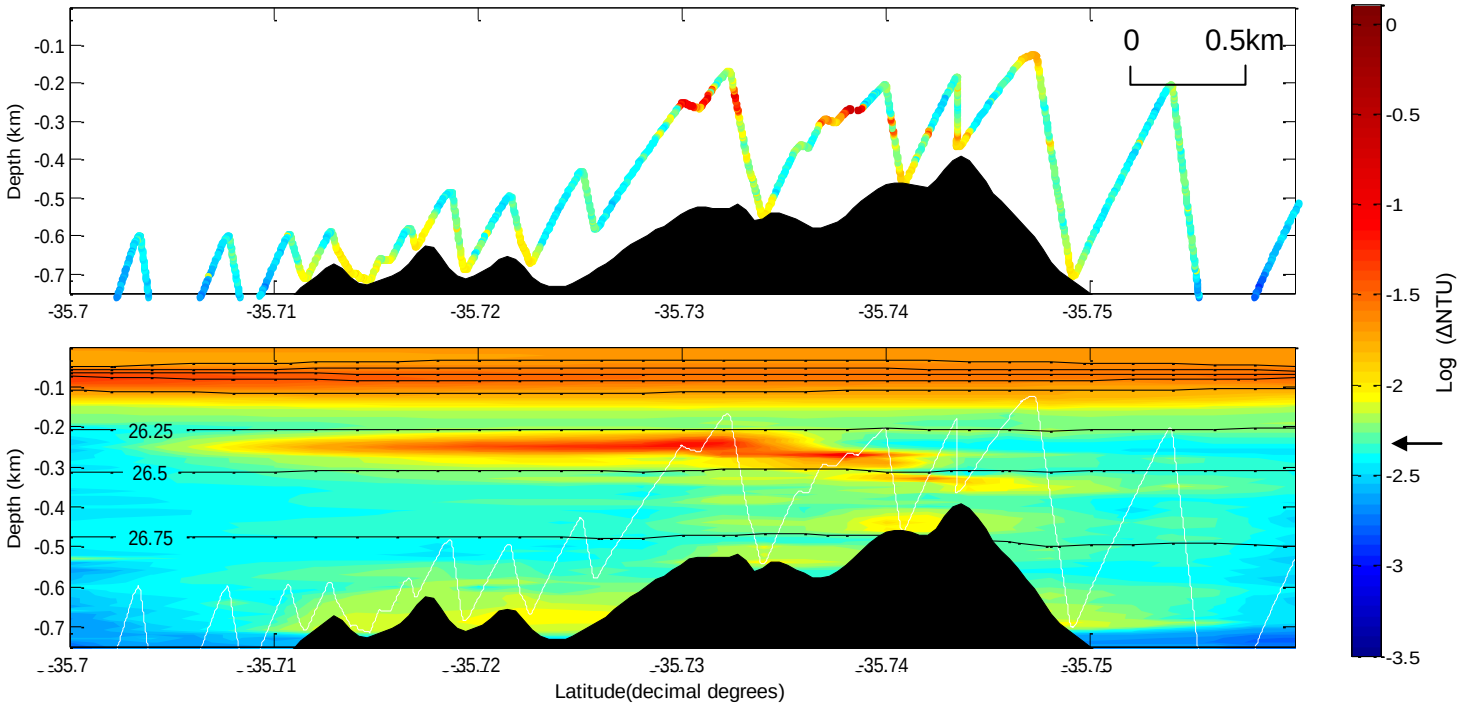

B) T09A06

C) T09A07

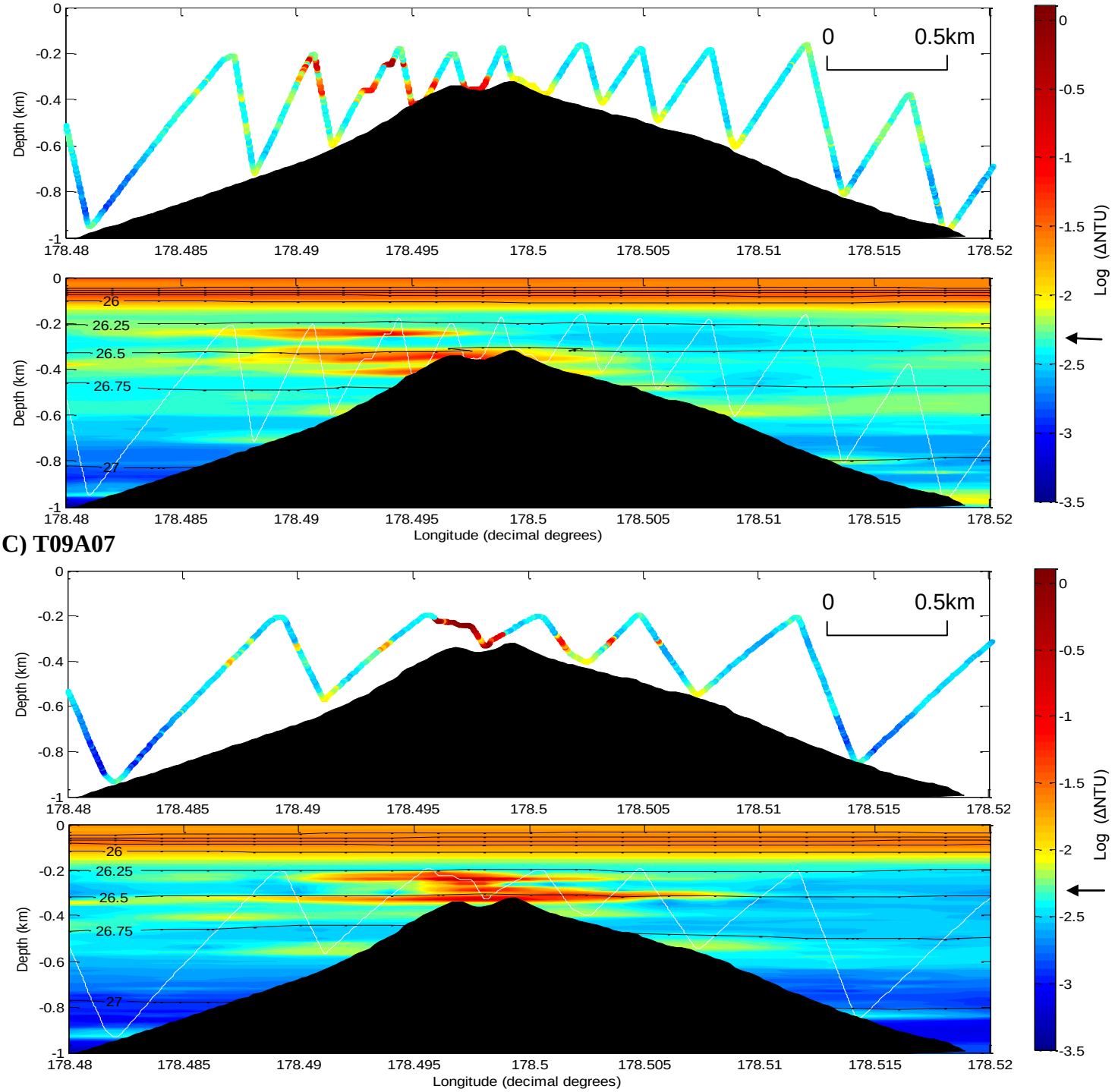

Figure 6: Zoomed in sections of CTD-O tow-yo transects carried out at Rumble III. A) Transect T09A05, carried out in a NW-SE direction, B) transect T09A06, carried out in a SW-NE direction during flood tidal currents, C) transect T09A07, a repeat of T09A06 but conducted during ebb tidal currents. Light-scattering measurements have been plotted as, log ΔNTU due to the wide range of light-scattering values that were measured. Typically a ΔNTU of 0.004 nephels (a log ΔNTU of -2.39) is a reasonable threshold for the plume boundary (Walker. S. L. pers. comm.), and is indicated by an arrow on the color scale. The upper panels display the measured light-scattering results, whereas the lower show extrapolation of these data. Lines of potential density have been plotted at 0.25 intervals, the CTD-O tow-yo track line plotted in white and underlying bathymetry (Dodge 2009) in black.

have been recorded here, advected by prevailing northwestward currents (Figure 5A). Although extrapolation of the tow-yo data agrees with the presence of the plume north of the summit, the extrapolation is not based on any physical current data and no conclusions can be drawn as to whether a plume exists here.

T09A06

The profile of T09A06 (Figure 6B) shows three distinct patches of high optical backscatter centered at about 245 m, 350 m and 420 m depth, to the west of the summit. A maximum ΔNTU of 0.655 nephels is apparent at a depth of 245 m. This shallow plume is associated with a potential density level of 26.35, but an elevated particle anomaly is present up to the 26.30 potential density level. The middle and deep plume layers are centered at potential densities of 26.55 and 26.63 respectively. The plumes spread to the east and west of their maximal centers at their level of neutral buoyancy, following isopycnals. The upper plume layer exhibits a rise height of about 60 m above the summit. Conversely the lower layer is located below the summit at a depth of 420 m on the western flank, suggesting a deeper source.

T09A07

The presence of a strong, more continuous plume layer over the summit is suggested by a large patch of high optical backscatter between 220 m and 330 m depth. The plume layers measured during T09A06 are still apparent, with centers at potential density levels, 26.30 and 26.54 respectively. The base of the plume layers lie 20m below the summit, and rise 110 m above the summit (Figure 6C). A high ΔNTU (1.11 nephels) was recorded at 242 m depth, with two smaller (but still high) peaks in ΔNTU of 0.89 and 0.68 nephels at 330 m and 220 m respectively. A raised optical backscatter signal at

about 420 m depth was also noted during T09A07 but a comparatively lower ΔNTU of 0.025 nephels, means this plume is dwarfed by the intense plume at a depth of 242 m.

Temperature and Salinity Anomalies

The maximum temperature anomaly of -0.38°C and maximum salinity anomaly of -0.11 were measured in T09A07 at a depth of 236 m, during the downcast at Rumble III summit (longitude 178.497 E on Figure 6C). Temperature and salinity anomalies were only apparent in this section of the tow where ΔNTU values were highest (Figure 7).

There is a strong relationship between temperature anomaly and ΔNTU for the region above the summit where high plume signatures were recorded (Figure 8A). Two trend lines have been plotted for temperature anomaly and ΔNTU data from T09A07 between potential density levels 26.0 and 26.6, see

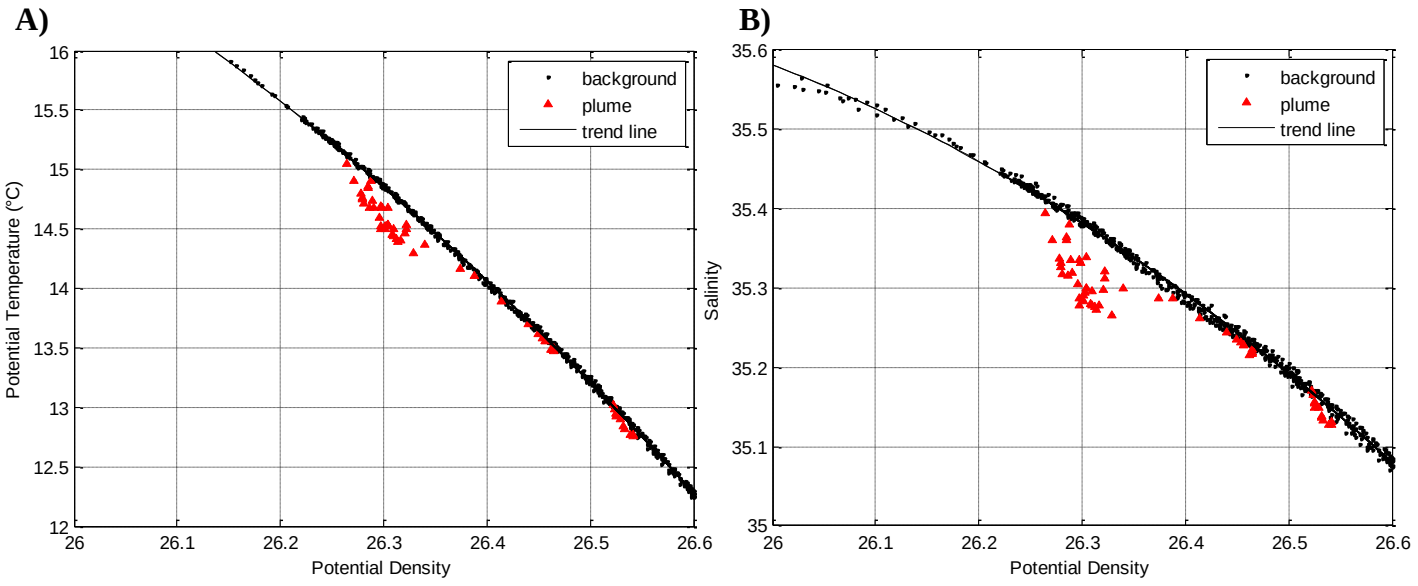

Figure 7: Relationship between potential density and A) potential temperature and B) salinity for T09A07. Large red triangles highlight regions with a hydrothermal plume signature (ΔNTU >0.1 nephels). The trend line was fit to the background data with ΔNTU <0.1 nephels. This value was chosen to isolate the stronger plume signals and exclude any small ΔNTU that may be due to sediment near the sea floor. The relationship was calculated for the density layer between 26 and 26.6, to isolate the regions of plumes and remove the upper thermocline layer. Potential density lines on Figure 6C show where this section of the tow occurs. The standard deviation of background values from the trend line (0.02°C) was calculated as a tool to determine significant temperature anomaly values.

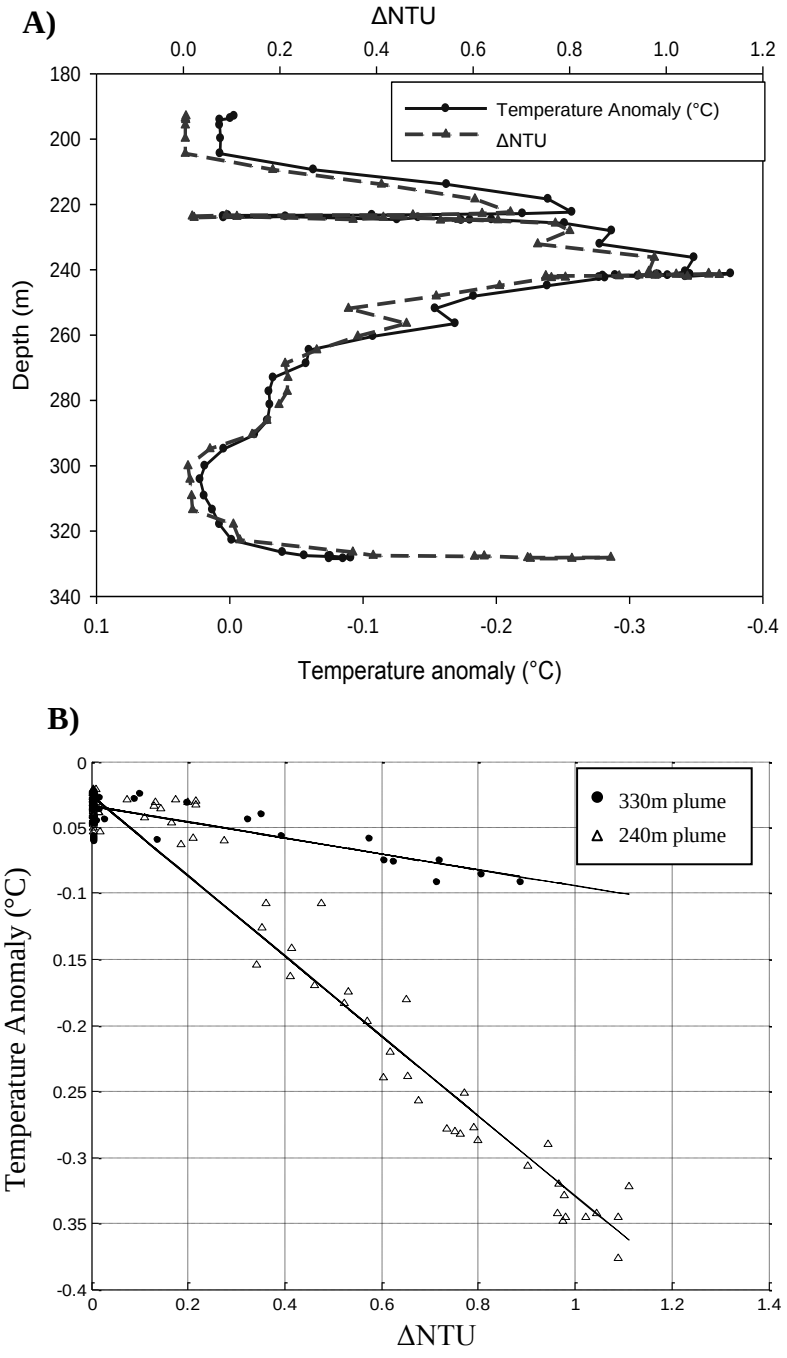

Figure 8: A) A comparison of ΔNTU and temperature anomaly (°C) with depth (m) for the section of strong plume anomalies detected over the summit of Rumble III during T09A07. B) Linear trends of temperature anomaly (°C) against ΔNTU for T09A07 for upper (240 m) and lower (330 m) plumes.

Figure 8B. Data points below 300 m have been used to compute the trend line for the 330 m plume and data points above 300 m for the 240 m plume. These depths were chosen based on Figure 8A. Linear regression analysis of temperature anomaly versus ΔNTU (Figure 8B) returns a correlation coefficient of -0.98 for the shallow plume and -0.80 for the deep plume, both with a >99% confidence. Only values with a temperature anomaly greater than the calculated error (0.02°C) were used to compute the trend line in order to test only data with a significant temperature anomaly. The same trend was detected with salinity anomalies in the region of maximum plume signal.

T09A06 showed a temperature and salinity anomaly of

-0.07°C and -0.02 respectively. However, temperature anomalies of this order were also noted near the seafloor in the absence of other indicators of hydrothermal plumes. Considering the strong background gradient and a standard deviation of 0.04°C calculated for this tow, these anomalies cannot be considered significant.

Results of camera tow surveys did not locate the source of venting at Rumble III and hence source conditions are not known. Camera tow surveys did however reveal temperature spikes of ~1°C at about 330 m and 420-460 m depth which imply proximity to a source of venting.

Computer Modeling

The discovery of a temperature anomaly within the plume region during T09A07, the recorded rise height of 125 m (see Appendix, Table 1), and bathymetry data provide some constraint on the characteristics of the venting source and estimates have be made here using the buoyant model of Speer and Rona (1989). Initially the vent source radius was fixed at a value of 0.1 m (Speer and Rona 1989) but early model simulations revealed that a source of this size could not produce the recorded rise height, even with unrealistically high (>500°C) source temperatures. Consequently source radius, source temperature and source depth were varied in model simulations to identify a range of potential source conditions that are consistent with field measurements. These trial and error experiments (see Appendix, Tables 2, 3 and 4), agree with other studies (Speer and Rona 1989) in that higher rise heights are obtained with a larger source radius and/or a greater source temperature. A source height of 330 m, just below the summit, was used for initial calculations based on the location of temperature spikes recorded during camera tow surveys. As Table 3 of the Appendix shows, increasing the source depth to 450 m did not yield the measured temperature anomalies. The measured anomalies were also not obtained assuming a source depth at the summit. Results are in agreement with Rudnicki and

Elderfield (1992) in that the same maximum rise heights and anomalies can be modeled based on different source radii. In this case a change in source radius is balanced by a change in source temperature so the buoyancy flux remains approximately the same.

A range of source conditions were consistent with measured plume characteristics, and judgments are made here based on past studies to suggest which are the most plausible for Rumble III. Modeling produced the most similar results for a source of venting at a depth of 330 m, with a temperature of 200-400 °C and radius of 0.22-0.33 m. These conditions constrain the buoyancy flux to a range of 4.5-4.9 x 10^{-2} m^4s^{-3}.

Calculations using the Middleton (1986) model for a plume in a crossflow show the effect of introducing a crossflow. Using the ambient potential density gradient at 330 m depth, a source temperature of 300°C, and a radius of 0.26 m (based on the modeling results above) the model predicts a rise height of 91 m in a crossflow of 0.15 m s^{-1}, and a rise of 83 m with 0.2 m s^{-1} crossflow. In no flow (using Speer and Rona's (1989) model) a rise height of 127 m is predicted.

Heat Flux

By constraining plausible vent source parameter ranges it was possible to estimate the heat flux at Rumble III using the calculated buoyancy flux,

$$Q = \frac{\rho c_p Bo}{g\alpha}.$$

Here Q is the heat flux and ρ is the density of the background water. The value for c_p (the specific heat capacity of water) has been taken from Rona and Trivett (1992) (4.5x10^{-3} J g^{-1} °C^{-1}) for a source temperature of 300 °C. Heat flux calculations based on exit conditions and the range of modeled

buoyancy flux of 4.5-4.9 x 10^{-2} m^4s^{-3}, indicate a heat flux of 107 $\pm$ 7 MW from a source of venting at 330 m (see Appendix, Table 2).

DISCUSSION

Plume Variability

Repeat transects at different stages of the tidal cycle, as well as data collected at Rumble III in the past 10 years, allow for different scales of variability to be examined. The results of this study provide strong evidence for variation of hydrothermal plume distribution on temporal scales of that of a tidal cycle. This makes it difficult to compare tow-yo results to previous years based on just one survey without knowledge of the background currents, especially considering that subtidal flow will also vary. Despite this, simple comparisons can be made.

The 2002 NZAPLUME II cruise noted plumes at about 250 m and 300 m (Walker. S. L. pers. comm.), whereas in 1999 plumes were detected at 170 m and 220 m (Baker et al. 2003), which shows some agreement with measured plumes between 200 m and 420 m during this study. In addition, the peak ΔNTU of 1.11 nephels recorded during T09A07 is the highest ever recorded at Rumble III, and is over an order of magnitude larger than the maximum of ~0.03 nephels recorded during the 2002 NZAPLUME II cruise (Walker. S. L. pers. comm.). Backscatter anomalies of this study indicate three patches of plumes located at different potential density levels, whereas past studies show two. The deep plume (420 m) could be a new feature or the location of previous surveys may have been such that this plume was missed. There is uncertainty as to the exact location of transects with respect to the source of venting and hence proximity to the core of the plume. The dramatic change in summit height that has occurred over the past 2 years of study at Rumble III suggests intense activity (Dodge 2009) and concurrent changes in source characteristics may explain altered plume distributions.

Short-term hydrothermal plume variability

Differences in optical backscatter values between repeat transects T09A06 and T09A07 display the inherent variability of hydrothermal plumes on time scale of tidal cycles. The optical data imply three plume layers centered at different levels of potential density. Rudnicki and Elderfield (1992), who noted layering in the plume structure at the TAG vent field on the Mid-Atlantic Ridge, offer three theories for this. First, the plume may be a broad plume which is divided into layers by convection within the plume, second, that there may be vertical diffusion from the neutrally buoyant plume, and third, multiple sources may be present. The plume layers in T09A06 appear quite distinct based on the ΔNTU with clear centers at 245 m, 350 m and 420 m depth. This is more consistent with multiple sources rather than convection or diffusion processes. T09A07 shows a more continuous plume structure extending from the summit of Rumble III to 200 m depth but layers are still discernible. If this pattern was caused by vertical diffusion of one large plume close to the summit, it seems unlikely that the strongest ΔNTU would occur 140 m away from the base of the plume. However, it is important to note the uncertainty in the exact location of the survey with respect to the plume core; strong particulate anomalies may have indeed occurred closer to the base of the plume in regions not surveyed. The different plume structure of T09A07 is perhaps indicative of the merging of plumes from different sources through mixing, convection and diffusion.

In addition to variability in the structure of the plumes, rise heights and levels of neutral buoyancy also varied. The shallow plumes of T09A06 and T09A07 were centered at different potential density levels (26.35 and 26.3 respectively) which correspond to a difference of ~20 m in the maximum rise height. The plume detected just above the summit in T09A06 and T09A07, is located at different depths (350 m and 330 m respectively) corresponding to the 26.55 and 26.54 isopycnals respectively. These differences in potential density are significant but it is important to consider the resolution of data when drawing conclusions. Potential density level estimates are made only where

there is measured data, as extrapolated data is disputable, but there is a limit to the accuracy of potential density level estimates, especially when plumes are broad and sampling points are sparse.

The fact that the plumes are equilibrating at different density levels on time scales as short as a tidal cycle highlights the dynamic and turbulent nature of hydrothermal plumes. The effects of background currents and source variability on hydrothermal plume distribution are discussed further in the following sections.

Background Currents

The currents recorded in the regions of plumes (0.15-0.2 m s^{-1}) were stronger than those typically associated with deep hydrothermal vent sites. For example, Garcia Berdeal et al. (2006) record a mean flow of 0.01-0.04 m s^{-1} at the Main Endeavour Field on the Juan de Fuca Ridge (situated at a depth of about 2200 m). The shallow site of Rumble III exposes the plume to high surface currents. Strong northwestward currents recorded during T09A06 are coincident with plumes to the west of the summit, whereas the plumes pass directly above the summit with the more northward currents of T09A07. Considering the strength of the measured currents, the change in plume location can be explained by the advection of the plumes with the tidally changing currents. It is possible that some of the measured lateral spread of the plumes is due to this advection. Studies using chemical tracers to measure the age of the plume would allow this hypothesis to be tested.

Background currents in the plume region were 0.15 m s^{-1}, 0.20 m s^{-1} and 0.15 m s^{-1} for T09A05, T09A06 and T09A07 respectively. Tows T09A06 and T09A07 are used here for comparison as they were carried out along the same transect line and hence some of the variability associated with location is avoided. T09A05 does however confirm the depths of the hydrothermal plumes at Rumble III. The lowest plume rise height (and highest potential density level of neutral buoyancy) was measured during

T09A06 when currents were strongest. Calculations using the Middleton (1986) model illustrate that plume rise height is decreased by 8 m when increasing background current velocity from 0.15 m s^{-1} to 0.20 m s^{-1} Considering the limited resolution of both optical data and current data it seems reasonable that variations in the background current field could explain the ~20 m change in level of neutral buoyancy of the shallow plume. It is also important to consider whether the currents recorded at the time of surveying are forcing the rise height of the plume or whether a time lag exists.

It is likely that changes in background currents also play a role in the small changes in the level of neutral buoyancy of the plume located at approximately 330 m depth. The detection of only a weak plume signal at 420 m during T09A07 means that the potential density level of neutral buoyancy is hard to accurately determine and subsequent comparison with the 420 m plume of T09A06 has not been made.

Source Variability

Temporal changes in the buoyancy flux at the source of venting on tidal time scales could also be responsible for the changes in plume rise height. As the source radius, source velocity and source temperature increase, the buoyancy flux increases and a greater rise height is attained. Results of computer modeling place constraints on the characteristics of the venting at Rumble III and provide additional evidence as to the major controls on plume variability. For simplicity, model simulations were based on a fixed initial velocity (taken from Speer and Rona 1989), however, Crone et al. (2006) note pulsating flow and tidal variations. Sensitivity analyses of this assumed source velocity value show that model runs with increased source velocity can produce the measured plume characteristics if balanced by decreases in source radius (Appendix, Table 4). Although this introduces greater

uncertainty into the source conditions, the calculated buoyancy flux only changes by 5% for these various source conditions and hence would not change heat flux values greatly.

The fact that buoyant plumes are known to integrate heat and chemicals from numerous vent sources (Rudnicki and German 2002) means it is plausible that multiple sources are fueling the rise of the plumes. Larger effective source radii, and hence source areas at Rumble III, are representative of a cluster of sources and give plume model predictions more consistent with measurements. Multiple vent chimneys at Rumble III are also consistent with arguments put forward here for the multiple plume layers discernible in tow-yo surveys. The different magnitudes of particulate anomalies in the plume layers suggest multiple sources of different particle forming potentials (Rudnicki et al. 1994). Variability in the activity of these multiple vents could account for some of the variability in rise height and particulate anomalies recorded between repeat transects of this study. Model results suggest a source of venting at 330 m for the shallowest plume of T09A07, but the fact that a deeper plume (420 m) was also measured provides strong evidence for the existence of an additional deeper vent source. Temperature spikes recorded during camera tow surveys at 440-460 m further support this hypothesis.

Temperature and Salinity Anomalies

The discovery of a cold, fresh plume signature aids the constraint of source conditions at Rumble III as a smaller range of conditions are consistent with both measured rise heights and measured temperature and salinity anomalies. Modeling experiments produce the recorded temperature anomalies for a range of source temperatures and radii. However, a modeled rise height of 126-128 m accompanies these initial conditions, which is 1-3 m higher than the measured rise of 125 m. This is the maximum predicted rise height and does not include effects of background currents which, as discussed, could explain changes of this magnitude.

Short-term hydrothermal plume variability

Although a range of source characteristics produced the observed anomalies (Figure 9), many of these conditions are not deemed realistic. Table 2 (see Appendix) illustrates that low source temperatures (100°C), can produce the measured temperature anomalies if the source radius is increased to 0.5 m. A source temperature of 100°C seems low when comparing to estimates of vent temperatures at nearby Brothers volcano ranging from 225 – 305°C (de Ronde et al. 2005). Temperatures >500°C are also not realistic considering maximum vent temperatures found to date of 407 °C (German et al. 2008). Case B of Figure 9 is therefore considered most representative of venting conditions at Rumble III volcano.

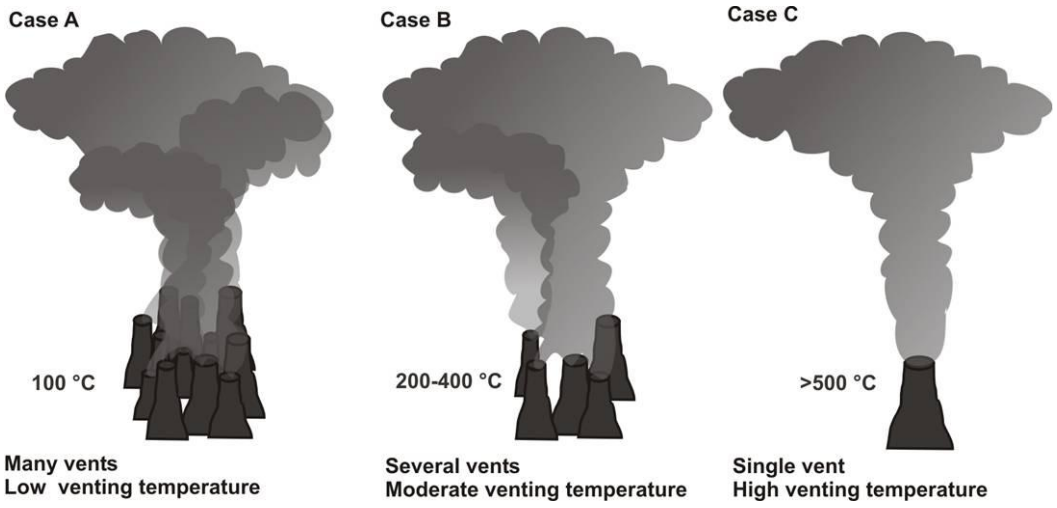

Figure 9: Schematic illustrating the different source characteristics that are consistent with measured plume distributions at Rumble III volcano. Of these three cases, case B is considered to be the most plausible (see text).

Another factor to consider when comparing field observations to model results is the assumptions made about the salinity of the ejected vent fluid. If in reality vent fluid is more saline, then model estimates would predict higher rise heights than those measured because of a reduction in buoyancy flux. Studies of vent fluid at the Endeavour segment of the Juan de Fuca Ridge document vent salinities that are similar to that of ambient seawater (Lupton et al. 1985). McDuff (1995) gives a range for stable vent sources from 20% of seawater, to roughly twice the seawater salinity. Coumou et

al. (2009) state that vent salinities are controlled by the source depth and the depth of the phase separation of seawater below the seafloor. Their results show that the bulk salinity of vent fluids increases with increasing pressure. This suggests that the vent fluid at Rumble III is likely to be towards the low salinity end of the range given by McDuff (1995) due to its shallow depth.

In the Speer and Rona (1989) model a 10% change in vent salinity results in a 1.6% change in rise height assuming an initial source temperature of 300°C and a source radius of 0.26 m. This error is small and decreasing source salinity to 10 only results in a 7% increase in rise height. The potential inaccuracy in the source salinity increases the error of model calculations, but without additional information on the vent source characteristics these assumptions are unavoidable. The model predictions of total source radius of 0.22-0.33 m and source temperature of 200-400°C are considered valid based on the available data, but accuracy is reduced by the uncertainty of assumptions. Further constraints on the source temperature require more accurate knowledge of the vent site at Rumble III, which await more extensive camera tow surveys or the use of a Remotely Operated Vehicle (ROV).

The magnitude of temperature and salinity anomalies varied between T09A06 and T09A07, being hardly distinguishable in T09A06. Both a steep and more gradual increase in negative temperature anomaly have been measured with increasing ΔNTU during T09A07 (Figure 8B). These two patterns have emerged due to the difference in temperature anomalies of plume centers at 220 m and 330 m. Although both areas are characterized by high optical anomalies, highly negative temperature anomalies (colder than -0.1°C) are only apparent in the upper plume layer. This may in part be due to the higher ΔNTU recorded in the upper plume layer, but may also reflect the presence of multiple vent sources of differing chemical characteristics. It is expected that temperature anomalies colder than -0.1°C should occur when ΔNTU exceeds 0.3 nephels (Figure 8B). Although this does not explain the small temperature anomalies detected in the deeper plume, it does offer an explanation as to

why temperature anomalies were not resolvable for T09A06 where ΔNTU values were typically below 0.2 nephels, except for one peak of 0.655 nephels at 245 m depth. ΔNTU of <0.03 nephels were recorded during the 2002 NZAPLUME II cruise (Walker. S. L. pers. comm.) and the results of this study indicate that temperature anomalies would not be expected (Figure 8B).

One possible explanation for the significantly higher ΔNTU and temperature anomalies of T09A07 is that the tow followed a recent strong plume event. Temporal variability in temperature anomalies brings forward the question of how long temperature anomaly signals last following a period of intense venting. T09A06 and T09A07 were separated temporally by 30 hours and it is possible that a burst of atypical (based on historic data) activity could have occurred in this time. More extensive surveying of the site and further repeat transects would provide information as to the permanency of the strong particulate signal. Anomalies from a mega plume event on the Carlsberg Ridge (the northern portion of the Indian Ridge system) have been traced a year after the event but were an order of magnitude lower (Ray et al. 2008). This could be due to a change in the source buoyancy flux, or the buoyancy frequency determined by the background stratification. It will be of interest to see whether future studies of Rumble III continue to detect elevated physical and chemical anomalies or whether these will reduce with time back to past values. The higher ΔNTU recorded during T09A07 could also be due to advection of the plume core such that the core was not recorded in T09A06. This highlights the limitations of plume surveys in knowing their exact location with respect to the spreading plume.

Heat Flux

Heat flux calculations based on exit conditions and the predicted buoyancy flux indicate a flux of 107 $\pm$ 7 MW from a source of venting 20 m below the summit of Rumble III (see Appendix, Table 2). Although the error range given here (based on the range of modeled buoyancy flux) is relatively

small, the cumulative errors from model assumptions are much greater. The range of source conditions that match measured plume distributions correspond to a small range in the calculated buoyancy flux, and it is this parameter that has been used for heat flux calculations. Heat fluxes are difficult to measure even when source data are available (Lupton 1995) and hence the degree of uncertainty of this calculation is high. The value calculated here is comparable to estimates of 500 ± 351 MW at the southern segment of the Juan de Fuca Ridge, but fluxes of 1700 ± 1100 MW have been estimated at the Endeavour segment (Bemis et al. 1993). The large error range of these fluxes highlights the difficulty of making accurate heat flux calculations.

Baker et al. (2003) made minimum estimates of the source heat flux (H_s) at Rumble III based on an estimated rise height (z^*) of 40 m in 1999. They computed a value of 3 MW, assuming a turbulent axially symmetric plume rising through a linearly stratified, motionless environment. This method gives an estimate of 317 MW based on the rise height and ambient water properties of this study. The difference in these estimates is predominantly due to the greater rise height (125 m) noted in this study and that $H_s \propto (Z^*)^4$ in the model used by Baker et al. (2003). A heat flux of 317 MW is however comparable to the 107 ± 7 MW calculated from buoyancy flux in this study. Ramondenc et al. (2006) note that the method used by Baker et al. (2003) is not reliable in the case where several vent sites contribute to the same coalesced plume. Also, the large power dependencies of the calculated heat flux on the rise height mean that small errors in rise height result in a large change in the heat flux. Calculations made using rise height, either directly or through buoyancy flux, inherently assume that the plume is reaching its maximum rise height and is not being pushed over by currents. Strong currents that reduce the rise height of the plume would therefore result in underestimates of the heat flux. Subsequently the estimates made here should only be considered accurate on an order of magnitude basis and serve to highlight the need for additional surveying at Rumble III. Estimates are

however more constrained than previous estimates by Baker et al. (2003), due to the discovered temperature anomaly. The thermal input to the oceans from hydrothermal venting is an area where data are lacking (Helfrich and Speer 1995) and hence even the first order calculations made here contribute to global ocean heat budget studies.

CONCLUSION

This study has found background current variability to be a likely contributor to the spatial variability of hydrothermal plumes, consistent with previous studies (Rudnicki and German 2002; Veirs et al. 2006). Modeling substantiates this, and despite model simplifications, results have been used in combination with field measurements to draw the following conclusions about the Rumble III hydrothermal vent site:

- Multiple plume layers exist above Rumble III, centered at ~220-245, 330-350, and 420 m.
- Hydrothermal plumes are advected to the north and northwest with changes in the direction of background currents due to tidal variation.
- Changes in background currents of 0.05 m s^{-1} between repeat tow-yo transects and short-term variability in source vent conditions could account for the 20 m change in rise height measured for the upper plume layers.
- Temperature anomalies can sometimes be detected in the region of the thermocline; an anomaly of -0.38°C was measured at 236 m during T09A07.
- Multiple vent chimneys are likely, with sites at both 330 m and depths greater than 420 m.
- Source temperature and combined source radius have been estimated allowing heat flux calculations of 107 ± 7 MW.

Short-term hydrothermal plume variability

The discovery of temperature and salinity anomalies at such a shallow submarine volcano supports increased investigation of these parameters at other shallow vent sites. Although high (perhaps atypically so) ΔNTU may be required for these anomalies to be resolved against strong background gradients, the potential to provide information about source characteristics and temporal variability should not be underestimated. These anomalies have allowed for further estimations of heat flux at Rumble III which enables improved estimates of the total heat flux over the entire Kermadec arc and of the hydrothermal contribution to the global ocean heat budget.

This study highlights the inherent variability of hydrothermal plumes and their distribution in the water column. Significant differences were measured on time scales of that of a tidal cycle, showing the need for caution when drawing conclusions about hydrothermal venting based on one snapshot of the plume. Short-term variation in both chemical and physical anomalies, as measured in this study, can lead to inaccuracies in calculations of, for example, heat flux or trace metal concentrations, at a particular site. Calculations based on rise height are likely to underestimate the hydrothermal heat flux where background currents are acting to push the plume over, and varying currents will lead to variable estimates of the heat flux. It is therefore recommended that where possible, future studies involve time series measurements, particularly when trying to determine the contribution of hydrothermal venting to global ocean budgets.

ACKNOWLEDGEMENTS

I would like to thank all the crew aboard *R.V. Thomas Thompson* for their technical support throughout the cruise. The team of New Zealand scientists, in particular Sharon Walker and Dr.Cornel de Ronde, made important contributions to this project, giving advice, sharing data, as well as aiding the smooth running of CTD-O tow-yos. Additionally University of Washington staff have provided

constant support and advice, helping with all aspects of the project from the planning to the processing of data. Professor Susan Hautala and Thomas Connolly provided Matlab scripts for model simulations and data processing and have solved numerous technical difficulties. I am extremely grateful for efforts of Professor Susan Hautala for her continual guidance and enthusiasm throughout the project. Thank you to Professor Rick Keil for leading the class and providing ukuleles for constant entertainment aboard the ship. Finally I would like to thank all my class mates for not only putting up with me on the cruise, but for their help and support before, during and after the cruise. Thank you everyone.

REFERENCES

Baker, E. T., R. A. Feely, C. E. J. de Ronde, G. J. Massoth, and I. C. Wright. 2003. Submarine hydrothermal venting on the southern Kermadec volcanic arc front (offshore New Zealand): location and extent of particle plume signatures, p. 141–161. *In* R.D. Larter and P.T. Leat [eds.], Intra-oceanic Subduction Systems: Tectonic and Magmatic Processes. Geological Society of London Special Publications, **219**.

Bemis. K. G., R. P. Von Herzen, and M. J. Mottl. 1993. Geothermal heat flux from hydrothermal plumes on the Juan de Fuca Ridge. J. Geophys. Res. **98:** 6351-6365.

Bonjean, F. and G. S. E. Lagerloef. 2002. Diagnostic model and analysis of the surface currents in the tropical Pacific Ocean. Journal of Physical Oceanography. **32**: 2938-2954.

Coumou, D., T. Driesner, P. Weis, and C. A. Heinrich. 2009. Phase separation, brine formation, and salinity variation at black smoker hydrothermal systems. J. Geophys. Res. **114**, doi:10.1029/2008JB005764, 2009.

Cowen, J .P., M. Bertram, S. Wakeham, R. E. Thomson, J. W. Lavelle, E. T. Baker, and R. A. Feely. 2001. Ascending particle flux from a hydrothermal plume: biogeochemical linkages with the upper water column. Deep-Sea Research I. **48**: 1093-1120.

Crone T. J., W. S. D. Wilcock, A. H. Barclay, and J. D. Parsons. 2006. The sound generated by mid-ocean ridge black smoker hydrothermal vents. PLoS ONE. **1**, e133, doi:10.1371/journal.pone.0000133.

de Ronde, C. E. J., E. T. Baker, G. J. Massoth, J. E. Lupton, I. C. Wright, R. A. Feely, and R. R. Greene. 2001. Intraoceanic subduction-related hydrothermal venting, Kermadec volcanic arc, New Zealand. Earth Planet. Sci. Lett. **193**: 359–369.

de Ronde, C. E. J., M. D. Hannington, P. Stoffers, I. C. Wright, R. G. Ditchburn, A. G. Reyes, E. T. Baker, G. J. Massoth, J. E. Lupton, S. L. Walker, R. R. Greene, C. W. R. Soong, J. Ishibashi, G.

T. Lebon, C. J. Bray, and J. A. Resing. 2005. Evolution of a submarine magmatic-hydrothermal system: Brothers Volcano, southern Kermadec Arc, New Zealand. Economic Geology. **100**: 1097-1133.

de Ronde, C. E. J., E. T. Baker, G. J. Massoth, J. E. Lupton, I. C. Wright, R. J. Sparks, S. C. Bannister, M. E. Reyners, S. L. Walker, R. R. Greene, J. Ishibashi, K. Faure, J. A. Resing, and G. T. Lebon. 2007. Submarine hydrothermal activity along the Mid-Kermadec Arc, New Zealand: Large-scale effects on venting. Geochem. Geophys. Geosyst. **8,** Q07007, doi:10.1029/2006GC001495.

Dodge, E. 2009. Catastrophic volcanic activity at Rumble III volcano based on EM300 bathymetry and direct seafloor imaging. Unpublished undergraduate thesis. University of Washington.

Egbert, G. D., and S. Y. Erofeeva. 2002. Efficient inverse modeling of barotropic ocean tides. J. Atmos. Oceanic Technol. **19**:183-204.

Garcia Berdeal, G., S. L. Hautala, L. N. Thomas, and H. P. Johnson. 2006. Vertical structure of time-dependent currents in a mid-ocean ridge axial valley. Deep-Sea Research I. **53**:367-386.

German, C. R., S. A. Bennett, D. P. Connelly, A. J. Evans, B. J. Murton, L. M. Parson, R. D. Prien, E. Ramirez-Llodra, M. Jakuba, T. M. Shank, D. R. Yoerger, E. T. Baker, S. L. Walker, and K. Nakamura. 2008. Hydrothermal activity on the southern Mid-Atlantic Ridge: Tectonically- and volcanically-controlled venting at 4–5°S. Earth Planet. Sci. Lett. **273**: 332-344.

Helfrich, K. R., and K. G. Speer. 1995. Oceanic hydrothermal circulation: Mesoscale and basin-scale flow. p. 347-356. *In* S. E. Humphris, R. A. Zierenberg, L. S. Mullineaux, and R. E. Thomson [eds.], Seafloor hydrothermal systems: physical, chemical, biological, and geological interactions. Geophysical Monograph, **91**.

Kelley, D. S., J. A. Baross, and J. R. Delaney. 2002. Volcanoes, fluids, and life in submarine environments. Annual Review Earth and Planetary Science. **30**: 385-491.

Lupton, J. E. 1995. Hydrothermal plumes: near and far field**,** p. 317-346. *In* S. E. Humphris, R. A. Zierenberg, L. S. Mullineaux, and R. E. Thomson [eds.], Seafloor hydrothermal systems: physical, chemical, biological, and geological interactions. Geophysical Monograph, **91**.

Lupton, J. E., J. R. Delaney, H. P. Johnson, and M. K. Tivey. 1995. Entrainment and vertical transport of deep-ocean water by buoyant hydrothermal plumes. Nature. **316**: 621-623.

Mcduff, R. E. 1995. Physical Dynamics of deep-sea hydrothermal plumes**,** p. 357-368. *In* S. E. Humphris, R. A. Zierenberg, L. S. Mullineaux, and R. E. Thomson [eds.], Seafloor hydrothermal systems: physical, chemical, biological, and geological interactions. Geophysical Monograph, **91**.

Middleton, J. H. 1986. The rise of forced plumes in a stably stratified crossflow. Boundary-Layer Meteorology. **36**: 187-199.

Morton, B. R., G. I. Taylor and J. S. Turner. 1956. Turbulent gravitational convection from maintained and instantaneous sources. Proc. R. Soc. Lond. A. **234**: 1–23.

Ramondenc, P. L. N. Germanovich, K. L. Von Damm and R. P. Lowell. 2006. The first measurements of hydrothermal heat output at 9°50′N, East Pacific Rise. Earth Planet. Sci. Lett. **245**:487-497.

Ray, D., I. H. Mirza, L. S. Prakash, S. Kaisary, Y. V. B. Sarma, B. R. Rao, Y. K. Somayajulu, R. K. Drolia and K. A. K. Raju. 2008. Water-column geochemical anomalies associated with the remnants of a mega plume: A case study after CR-2003 hydrothermal event in Carlsberg Ridge, NW Indian Ocean. Current Science, **95**: 355-360.

Rona, P. A. and K. G. Speer. 1989. An Atlantic hydrothermal plume: Trans-Atlantic Geotraverse (TAG) area, Mid-Atlantic Ridge crest near 26°N. J. Geophys. Res. **94**: 13879-13893.

Rona, P. A. and D. A. Trivett. 1992. Discrete and diffuse heat transfer at ASHES vent field, Axial Volcano, Juan de Fuca Ridge. Earth Planet. Sci. Lett. **109**:57–71.

Rudnicki, M. D. and H. Elderfield. 1992. Theory applied to the Mid-Atlantic Ridge hydrothermal plumes: The finite-difference approach. J. Volcanol. Geotherm. Res. **50**: 161–172.

Rudnicki, M. D., R. H. James and H. Elderfield. 1994. Near-field variability of the TAG non-buoyant plume, 26°N, Mid-Atlantic Ridge. Earth Planet. Sci. Lett. **127**:1-10.

Rudnicki. M. D. and G. R. German. 2002. Temporal variability of the hydrothermal plume above the Kairei vent field, 25°S, Central Indian Ridge. Geochem. Geophys. Geosyst. **3**, doi:10.1029/2001GC000240.

Speer, K. G., and P. A. Rona. 1989. A model of an Atlantic and Pacific hydrothermal plume. J. Geophys. Res. **94**: 6213-6220.

Tomczak, M., J. S. Godfrey. 1994. Regional Oceanography: An introduction, first edition. Elsevier Science Ltd.

Turner, J.S. 1973. Buoyancy Effects in Fluids. Cambridge University Press.

Veirs, S. R., R. E. McDuff, and F. R. Stahr. 2006. Magnitude and variance of near-bottom horizontal heat flux at the Main Endeavour hydrothermal vent field. Geochem. Geophys. Geosyst. **7**, doi:10.1029/2005GC000952.

Walters, R. A., D. G. Goring, and R. G. Bell. 2001. Ocean tides around New Zealand. New Zealand Journal of Marine and Freshwater Research. **35**: 567-579.

Wilson, C., J. L. Charlou, E. Ludford, G. Klinkhammer, C. Chin, H. Bougault, C. German, K. Speer and M. Palmer. 1996. Hydrothermal anomalies in the Lucky Strike segment on the Mid-Atlantic Ridge (37’17’N). Earth Planet. Sci. Lett. **142**: 467-477.

Wright, I. C. 2001. In situ modification of modern submarine hyaloclastic/pyroclastic deposits by oceanic currents: an example from the Southern Kermadec arc (SW Pacific). Marine Geology. **172**: 287–307.

APPENDIX

Table 1: Measured characteristics of hydrothermal plumes at Rumble III during T09A06 and T09A07 with an assumed vent source at 330 m just below the summit of Rumble III.

	T09A06	T09A07
Maximum rise height (depth) of plume (Z_{max}) (m)	100 (230)	125 (205)
Height (depth)of maximum anomaly (Z_{anom}) (m)	85 (245)	94 (236)
Temperature anomaly (°C)	-0.07	-0.38
Salinity anomaly	-0.02	-0.11

Table 2: Modeled characteristics of hydrothermal plumes above Rumble III based on calculations using the Speer and Rona (1989) buoyant plume model. The height of neutral buoyancy has been determined based on where plume density is equal to ambient density. Where model calculations are consistent with measured plume characteristics, values have been highlighted in bold and buoyancy flux (m^4s^{-3}), and heat flux (MW) have been calculated. Calculations have been carried out based on a source depth of 330 m, for a range of source temperatures (T_0) and total source radius.

Total source radius (m)	Max rise height (m)	Height of neutral buoyancy (m)	Temperature anomaly at Z_{anom} (°C)	Salinity anomaly at Z_{anom}	Buoyancy flux (m^4s^{-3})	Heat flux (MW)
T_0 = 100°C						
0.4	116	87	-0.50	-0.10		
0.5	**128**	**92**	**-0.38**	**-0.10**	**5.3×10^{-2}**	**124**
0.6	140	102	-0.26	-0.10		
T_0 = 200°C						
0.3	122	90	-0.43	-0.10		
0.4	140	102	-0.25	-0.10		
0.35	131	121	-0.34	-0.10		
0.33	**128**	**92**	**-0.38**	**-0.10**	**4.9×10^{-2}**	**114**
T_0 = 300°C						
0.2	112	85	-0.52	-0.10		
0.25	124	91	-0.41	-0.10		
0.3	136	100	-0.29	-0.10		
0.26	**127**	**92**	**-0.38**	**-0.10**	**4.7×10^{-2}**	**106**
T_0 = 400°C						
0.2	120	90	-0.44	-0.10		
0.25	134	99	-0.31	-0.10		

Table 2 continued:

Total source radius (m)	Max rise height (m)	Height of neutral buoyancy (m)	Temperature anomaly at Z_{anom} (°C)	Salinity anomaly at Z_{anom}	Buoyancy flux (m^4s^{-3})	Heat flux (MW)
T_0 = 400°C						
0.3	147	109	-0.17	-0.10		
0.22	**126**	**92**	**-0.39**	**-0.10**	**4.5×10^{-2}**	**100**
T_0 = 500°C						
0.1	94	71	-0.69	-0.11		
0.2	**127**	**92**	**-0.37**	**-0.10**	**4.7×10^{-2}**	**102**
0.3	156	115	-0.06	-0.10		

Table 3: As for Table 2 but with source depths of 450 m and 310 m. Although a rise height of 245 m and 105 m respectively, (required to match field measurements) can be produced, the modeled temperature and salinity anomalies are not consistent with field measurements, and hence heat flux and buoyancy frequency have not been calculated.

Source depth (m)	Total source radius (m)	Max rise height (m)	Height of neutral buoyancy (m)	Temperature anomaly at Z_{anom} (°C)	Salinity anomaly at at Z_{anom}
T = 200°C					
450	0.8	219	170	-1.27	-0.20
450	1.0	238	182	-1.11	-0.20
310	0.2	99	71	-0.34	-0.08
310	0.25	110	80	-0.22	-0.08
T = 300°C					
450	0.7	226	176	-1.20	-0.20
450	0.8	238	182	-1.10	-0.20
450	0.9	249	193	-1.00	-0.20
310	0.1	79	61	-0.51	-0.08
310	0.2	110	80	-0.22	-0.08
310	0.3	136	99	0.11	-0.08
T = 400°C					
450	0.7	240	184	-1.08	-0.20
450	0.8	253	196	-0.97	-0.19
310	0.15	103	74	-0.29	-0.08
310	0.2	119	89	-0.11	-0.08
T = 500°C					
450	0.6	237	181	-1.1	-0.20
450	0.7	252	195	-0.98	-0.19
310	0.1	90	68	-0.42	-0.08
310	0.2	127	94	-0.01	-0.08

Table 4: As for Table 2 but with varying source velocity and source radius.

Total source radius (m)	Source velocity(m)	Max rise height (m)	Height of neutral buoyancy (m)	Temperature anomaly at Z_{anom} (°C)	Salinity anomaly at at Z_{anom}	Buoyancy flux (m^4s^{-3})
T_0 = 300°C						
0.25	0.2	106	81	-0.58	-0.10	2.2×10^{-2}
0.25	**0.4**	**124**	**91**	**-0.41**	**-0.10**	**4.3×10^{-2}**
0.25	0.8	148	110	-0.16	-0.10	8.7×10^{-2}
0.18	**0.8**	**125**	**91**	**-0.40**	**-0.10**	**4.5×10^{-2}**
0.25	1	156	115	-0.06	-0.10	10.8×10^{-2}
0.1	1	101	78	-0.62	-0.10	1.7×10^{-2}
0.16	**1**	**125**	**91**	**-0.40**	**-0.10**	**4.4×10^{-2}**